

Received 3 April 2024, accepted 3 June 2024, date of publication 13 June 2024, date of current version 28 June 2024.

Digital Object Identifier 10.1109/ACCESS.2024.3414345



RESEARCH ARTICLE

Leg Joints Angle Estimation During Walking Using the Motion of the Posterior Superior Illiac or **Greater Trochanter Points**

MAHDY ESLAMY^[0] AND MO RASTGAAR^[0], (Senior Member, IEEE) ¹School of Computing, Engineering and Digital Technologies, Teesside University, TS1 3BX Middlesbrough, U.K.

²Purdue Polytechnic Institute, Purdue University, West Lafayette, IN 47907, USA

Corresponding author: Mahdy Eslamy (m.eslamyatgmail.com)

This work was supported by the National Science Foundation (NSF) under Grant 1921046.

ABSTRACT Estimation of the trajectories of the leg's joints is of importance in gait studies, as well as in the design of motion planners and high-level controllers for exoskeletons, orthotics, prosthetics, and humanoid robots. Human locomotion is a harmonic phenomenon which benefits from collaboration between different parts of the leg. This collaboration, together with taking into account the natural hierarchy in the human body structure, necessitates paying attention to the fact that the motions of the legs' lower limbs are influenced by the motions of the upper ones. Having this point and its potential consequences in mind, this study aims to create a relationship between the legs' joints, and the motion of the posterior superior illiac (PSI) or great trochanter (GTR) points, separately. From anatomical point of view, both of the points are above the ankle, knee, and hip joints. To continuously map the inputs to the outputs, without requiring switching rules, speed estimation, gait percent identification or look-up tables, a nonlinear auto-regressive modeling with wavelets and neural network is used. The proposed approach is investigated for forty-two subjects at different walking speeds. The method is tested for six case studies, in which their root mean square (RMS) errors, mean absolute errors (MAEs) and correlation coefficients ρ_{cc} are compared. The results show that using GTR point leads to higher estimation accuracy. For instance, in one of the testing case studies, ρ_{CC} were 0.97, 0.95, 0.91 using GTR point, in comparison to 0.95, 0.93, 0.87 using PSI point, for the hip, knee, and ankle joints, respectively. A similar trend was also observed for root mean squared errors (RMSE) and mean absolute errors (MAEs). In addition, it is found that highest performance occurs in hip angles estimation, and least performance is seen for the ankle joint. Furthermore, the impact of using both velocity and acceleration inputs on the estimation accuracy is also investigated. The results show that using velocity or acceleration of the GTR or PSI inputs leads to relatively similar results. Nonetheless, the results related to the GTR point are in general better. The impacts of using both velocity and acceleration inputs as well as different estimator functions (such as sigmoid function) are also investigated and discussed.

INDEX TERMS Estimation of the leg joints' angles, gait analysis, posterior superior illiac or greater trochanter, controller design, prosthetics, orthotics.

I. INTRODUCTION

Aside from designing compact and versatile orthotics, prosthetics, and exoskeletons, which is a major design challenge, the other challenge is related to their intelligence, i.e., how to set their operation in line with a human user's locomotion. High accuracy intent recognition is

The associate editor coordinating the review of this manuscript and approving it for publication was Mohammad Zia Ur Rahman.

usually required, but remains challenging, since human locomotion is the result of intricate interactions between brain, spinal cord, muscles, limbs, and joints. Using sensory inputs from all of those potential sources would result in computationally complex control algorithms as well as complicated mechanical systems. Therefore, the research community has focused to develop methods to control these devices using as minimum sensory inputs as possible.



In the following, different motion planning methods that are proposed to predict the motion of the biological or prosthetic lower extremity joints will be discussed.

A. PREVIOUS STUDIES: THEIR ESTIMATION ALGORITHMS AND FINDINGS

One early method was to use the motion of the sound side, and then imitate it on the amputated side. This "echoing" algorithm was proposed to control a prosthetic knee [1]. Two main disadvantages of this method were, requiring to instrument the sound side, and, the delayed repetition of sound side's motion. The method was later improved through complementary limb motion estimation (CLME) algorithm [2]. In the latter, although using sound side's motion, the state estimation was performed without delay.

Ankle joint's motions were estimated using speeds and gait percents in [3]. For this purpose, shank angular positions and velocities were used to extract corresponding speed and gait percent based on phase plane concept. Next, an off-line saved look-up table was used to find out the corresponding ankle angles. To estimate speeds, the method however required if-then decision making. A similar approach was later used to estimate knee angles [4]. Thigh angle and its integral were used for gait percent estimation. Next, the knee angles were expressed as a function of the derived gait percents using the Fourier transform. The work was later improved to take into account different speeds and gaits, using basis and task functions [5], [6]. The main advantage over [3] was that, in [5], [6] a functional approach was adopted, as opposed to the table-based approach proposed by the former.

Seven regression algorithms were used to compare leg joints' angle estimation in [7]. To do so, foot angular velocities and translational accelerations (at heel) were used to predict sagittal plane ankle, knee, and hip angles at a self-selected walking speed. The comparisons showed that generalized regression neural network (GRNN) algorithm had the best performance. A similar algorithm was used to estimate sagittal plane hip, knee, and ankle angles using foot and shank 3D angular velocities and linear accelerations (twelve signals) in [8]. The GRNN was combined with the Fourier transform to estimate leg joints' angles in [9]. The work used anthropometric parameters such as foot, shank, and thigh lengths, together with cadence and stride length.

Shank angular positions and velocities were employed to predict ankle joint angles at various walking speeds in [10]. The work was later continued to predict knee angles using thigh angular positions and velocities [11]. In both works, Gaussian regression was employed to predict joints' angular positions. In another work, thigh angles and linear accelerations were utilized to estimate gait percents and speeds [12]. Next, the corresponding knee angles were predicted for various walking speeds based on an off-line look-up table. To lessen the number of the inputs, a nonlinear auto-regressive model with exogenous inputs was proposed to estimate ankle and knee angles [13]. To do so, only shank or only thigh angular positions were used (as

inputs) for estimations. The method had acceptable results in comparison to different studies.

EMG signals from semitendinosus, vastus lateralis, rectus femoris, and vastus intermedius were used to predict knee positions in the sagittal plane in [14]. To classify different patterns, a Levenberg-Marquardt multi-layer perceptron neural network was used. In another study, tibialis anterior, gastrocnemius, and soleus signals were utilized to predict ankle angles, using two different models [15]. First, a biomimetic model was proposed based on muscle properties such as muscle stiffness and damping factors, activation level, and isometric length. In the second modeling, a standard backpropagation algorithm was used to a train a feed-forward neural network. Both methods were able to estimate ankle motions with acceptable accuracy.

Ankle flexor and extensor signals were used to estimate ankle joint angles in [16]. A nonlinear autoregressive neural network was proposed whose activation functions were tansig and a linear function with unit slope. Using a similar methodology, ankle angles were estimated using tibialis anterior and gastrocnemius signals [17]. In another study, EMG signals from ten leg muscles were used to estimate ankle, knee, and hip angles [18]. It was shown that using a deep belief network was better than a principal components analysis approach [19] to extract features from surface EMG signals. Different studies showed that merging EMG signals and kinematics data (e.g., joints' angular positions or velocities) can potentially lead to more accurate results in comparison to using only EMG signals [20], [21], [22].

B. LIMITATIONS AND CHALLENGES OF MOTION PLANNING ALGORITHMS

As reviewed, different methods have been proposed for the estimation of the leg joints' angles (or moments). However, there are a number of issues that need more attention.

First, several studies have proposed estimation methods that can be used for human gait analysis, but would be less useful for motion planning of orthotics or prosthetics. For example, foot motion was used for ankle angle estimations in [7]. This approach cannot be used to control a transtibial prosthesis, since in this circumstance the biological foot is missing, and therefore no information can be obtained from it. Or, knee joint positions were estimated using inputs obtained from shank and thigh [23]. Since knee joint is between the shank and thigh, in case of a transfemoral amputee with a missing shank, this method can not be used, as inputs coming from biological shank would be missing. Lot of works related to the joints' angle/moment estimation can be put in this category.

Thigh motion together with other inputs were used to high-level control a hip orthosis in [24], or hip angles were used to estimate hip moments for a hip orthosis in [25]. While the methods worked, obtaining inputs from a point which is below the desired joint, might result in a paradoxical condition for the intent recognition by the high-level controller. In other words, it does not seem *logical* to



use the inputs from a limb, and then trying to estimate what the same limb "should" do at the same time.

In the above example, the inputs (coming from thigh) are already "directly" influenced by the motion of the hip orthosis. Therefore, it might not be a good idea to "use" the motion of the thigh, and to *simultaneously* estimate what it should do (desired motion). In this example, thigh motion can be used in a low-level controller in hip orthosis, e.g., in its PD controller, to adjust its motions. However, using its motion for intent recognition of the same joint may not be logical. Therefore, the authors believe that the desired setpoints (i.e., the desired output angles/moments) should be generated based on *another* less-influenced input source.

The second issue is related to the number of the input sources that are to be used in an estimation algorithm. While using diverse sources might potentially lead to more accurate controller, using less inputs (i.e., designing minimal-sensory controllers) should be the first target. When the limitations and strengths of a minimal-sensory algorithm are identified, the use of more input sources into the algorithms can be better justified. Unfortunately, lots of the studies use a number of pre-selected input sources without explaining whether all of them were really required or not.

Third, the vast majority of the controllers for active powered prosthetics/orthotics rely on the finite state machine (FSM) approach [26], [27]. In this approach, the gait cycle is divided into different sections (states) according to the gait events, and for each section a control rule is devised. Furthermore, switching rules are also required to transit between the states. In contrast, human gait seems, at least visually, a continuous seamless event. This is a good motivation for trying to develop continuous motion planners.

C. THE CONTRIBUTIONS OF THIS STUDY

This study is designed to address some of the abovementioned issues, to the places possible. *First*, our study aimed to pay attention to the natural hierarchy in the human body. Therefore, the motion of a specific joint is estimated through inputs coming from a point above it. Such an attitude can potentially be more logical and constructive, as previously discussed.

Since this study is also targeting the hip joint, it was decided to use input source(s) close to, but above this specific joint. One potential candidate point could be around the waist. To do so, two points were of interest. Specifically, the motion of the posterior superior iliac point (PSI, on the waist), and separately, that of the greater trochanter (GTR, on the connection point of the hip joint), is used to estimate ankle, knee, and hip angular positions during walking.

GTR point is in the region close to the thigh (hip) rotation axis, and PSI point is close to the points used in [28] and [29]. The selected two points are close to the human center of mass [30]. The excursion of the center of mass is used for a wide spectrum of inspections, from gait energetics to gait quality, which show its importance in human gait analysis [31], [32], [33], [34], [35], [36]. Despite its wide use in gait

studies, little has been devoted to leverage its motion in high-level controlling and motion planning of prosthetics or orthotics. Aside from this matter, human locomotion seems harmonic which implies constructive interactions between different joints and limbs of the lower extremity. The effect of these interactions might be summarized in the motion of the center of mass [37], [38], or possibly those two proximal points. This study aims at investigating this matter by inspecting the opposite, i.e., if motions of those two points could be converted to the motions of the leg joints, paving the way for a potential motion planner for prosthetics or orthotics.

Vertical ground reaction forces were estimated using three IMUs in [28]. One of them was attached to the lower trunk on the fifth lumbar vertebra. The study showed that the forces can be estimated with high accuracy using only one wearable sensor mounted at the waist. In a relatively new study, leg joints' angles were estimated using five IMUs attached to pelvis, thighs and shanks [29]. A deep learning model with convolutional and recurrent layers was used for estimation of the joints' angles in twenty-seven subjects while walking and running on a treadmill. To predict leg joints' angles (stance and swing phases separately), moments (stance phase), and ground reaction forces, a sacrum-attached IMU was used in [39]. The inputs were acceleration, velocity, displacement and time, and the proposed approach was investigated on seven subjects.

Second, this study aims to design a minimal-sensory motion planner. As mentioned previously, only when limitations and strengths of such an approach are investigated, the use of more input sources can be better explained. To do so, different scenarios are planned and compared which will be discussed in full detail in the Methods section.

Third, the estimations are performed continuously, and directly, from inputs to the estimated outputs. This attitude helps avoid the intermediate steps such as gait percent identification, look-up tables, switching rules, or speed estimation. The motivation behind this approach is that such parameters are usually derived from the already available sensory information or obtained from an extra source [3], [4], [5], [40]. Thus, it is aimed to create a direct mapping from inputs to the outputs.

Fourth, since those two points are used (separately) to estimate sagittal plane ankle, knee and hip joints' positions, this enables to relate all of the positions to a single point on the human body, and to pave the way to develop motion planners that can be used as high-level controllers for smart orthotics, prosthetics, or exoskeletons. This approach would be potentially useful to take steps towards a more comprehensive controller for such devices.

In addition to the above, studies usually use data from participants that are within a similar age range, and usually from young population. Although it is a reasonable starting point for human gait analysis and designing high-level controllers, it would also be logical to analyze the developed methods for a wide range of age which involves both young and old participants. This approach can lead to more

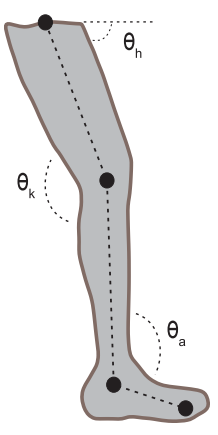


FIGURE 1. Schematic view for the definition of the hip angle θ_h , knee angle θ_k , and ankle angle θ_a , as well as positions of some of the markers used in this study. See Methods for more detailed information.

comprehensive analysis, and therefore, in this study a data-set obtained from participants within a *wide* age range was used.

To estimate leg joints' positions (outputs) in this study, a nonlinear autoregressive model [41], [42] together with wavelets is used to create a direct mapping between the inputs (the motions of the PSI or GTR points) and the outputs, hence circumventing the need to define intermediate parameters (for instance, gait percents).

Reminiscent of the Fourier series, a signal is converted into a number of small waves (the wavelets) in the wavelet theory. The wavelets, which wax and wane through time, have however an underlying difference in comparison to the basis functions in Fourier series (the "open-end" sine and cosine functions). Human gait has a periodic as well as variable nature. Wavelets can follow changes in a system's response both in time and frequency [43], [44], [45]. It enables them to express a part of function with a resolution corresponding to its scale. The Fourier functions can not describe a function properly enough when the frequency changes with respect to time (which is common in human gait studies) or when local fluctuations exist at some points of the function to be estimated. These features make the wavelets a better choice [46] in comparison to expressing functions using DFT (discrete Fourier Transform). Full details are provided in the next sections.

The structure of the paper is as follows: at first the fundamentals and methods of the investigation are explained, next results are reported and then explained and discussed, and at the end, different conclusions are made regarding the findings of the study and how they compare with other studies. Furthermore, the impact of this study and application implications are also discussed.

II. METHODS

A. DATA ACQUISITION AND REQUIRED PROCESSING

The motion of the right posterior superior illiac (PSI) and greater trochanter (GTR) points are separately used in this work to estimate ipsilateral ankle, knee, and hip angles (in sagittal plane). The former point lies on the waist, and the

latter lies at the intersection of the hip joint and leg. The definitions of the angles $(\theta_h, \theta_k, \text{ and } \theta_a)$ are shown in Fig. 1.

Throughout this work, the publicly available data-set discussed in [47] was used. The set contained data for 42 subjects at eight different speeds (slow, comfortable, and fast, from 0.4 m/s to 2.2 m/s, depending on the subjects) walking on an instrumented treadmill (FIT, Bertec, Columbus, OH, USA, 300 Hz). Since each participant had its own range of speeds, the exact values of the speeds were different depending on each subject [47]. The dataset involved participants from 21 to 84 yrs old. This makes it a valuable set in order to analyze the impact of an estimation algorithm for a very wide age range. The data-set involved twenty-eight marker trajectories obtained from different human body's landmark points using a twelve-camera motion capturing system at 150 Hz [47].

To obtain (right) joints' angles, the relevant marker trajectories available in the aforementioned database were utilized. For this purpose, an extensive Matlab code was written to read the trajectories of desired markers. To obtain ankle angles, the trajectories of the fifth metatarsal, ankle, and knee markers were used (see Fig. 1). To obtain knee angles, the trajectories of the ankle, knee, and great trochanter markers were used. To obtain hip angles, the trajectories of knee and greater trochanter markers were used. Next, using triangular algebra, the marker trajectories were converted into joints' angles. This procedure was done for each subject, as well as, each speed under investigation. In addition, the marker trajectories of the (right) posterior superior iliac spine (PSI) and greater trochanter (GTR) were also extracted from the database, since these are the inputs to the estimation process. At the end of the processing, the quality of the data of each participant was investigated to ensure correct data is provided to the estimation algorithm. The general shape of the obtained data was verified against [48] to ensure the data are bio-mechanically acceptable. An exact comparison was not possible nor logical, since each human subject has its own walking behavior.

B. THE ESTIMATION ALGORITHM

As mentioned in Introduction, to estimate θ_h , θ_k , and θ_a (i.e., the estimated *outputs* \hat{y}), a nonlinear autoregressive model was used [41], [42]. In this regard, a function relationship f can be defined which relates the input x to the output y as y = f(x) or $\hat{y} = \hat{f}(x)$, where \hat{y} is an estimation of the actual y. Different function estimators can be used in nonlinear autoregressive modelling technique (see Fig. 2). The pool contains candidate functions such as wavelets, polynomials or sigmoids, or a weighted sum of those functions, e.g., in the form of a network [46], [49], [50] (Fig. 2). While it is out of the scope of this work to analyze *all* of the possibilities, it is the target of this study to concentrate on one possibility that can work. It was shown in a previous study that the weighted sum of the wavelets can be suitable candidate for biomechanical applications [13]. Accordingly, the function



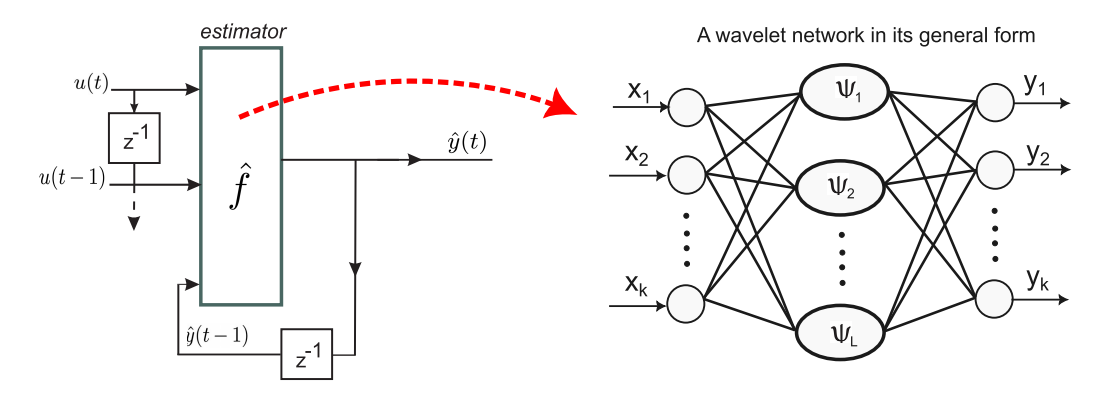


FIGURE 2. The general structure of the estimation algorithm using nonlinear autoregressive model with exogenous inputs. The left section shows the input for a case when $x(t) = [\hat{y}(t-1), u(t), u(t-1)]$. The estimator $\hat{f}(x(t))$ then processes the input to produce the estimated outputs $\hat{y}(t)$. The symbol ψ denotes a wavelet.

estimator \hat{f} can be written as $\hat{f}(x) = \sum_{i=1}^{L} \omega_i \psi_i(x)$, where ψ_i 's denote the wavelets (Fig. 2).

The input variable x can contain the current value of the input signal and/or its past values. In addition, it can take in the previous values of the outputs. Therefore, at time instance t, the general form of the input–output relationship would be $\hat{y}(t) = \hat{f}(x(t))$ in which x(t) = [y(t-1), y(t-1)]2), ..., u(t), u(t - 1), u(t - 2), ...]. The model order (i.e., how many current and past samples were used in x, and the components of x (kinematics, kinetics, EMG, etc) can vary depending on the problem to be solved [42], [51], [52]. The general structure of the estimation algorithm using nonlinear autoregressive model is shown in Fig. 2. The wavelets are represented by a number of basis functions [43], [44], [46]. Gaussian derivatives family (represented by the general formula $h(x) = ce^{-\frac{xx^T}{2}}$) [53] are suitable candidates for biomechanical studies [54], [55], [56], [57], [58].

C. INPUTS TO THE ESTIMATION ALGORITHM

In this study, for the input x different variations were investigated. To do so, three main variants of x were considered which involved velocity and/or acceleration information: 1) when $x = [\dot{z}_{psi}]$, 2) when $x = [\ddot{z}_{psi}]$ and 3) when $x = [\dot{z}_{psi}, \ddot{z}_{psi}]$. The variable \dot{z}_{psi} denotes the vertical velocity of PSI (with respect to the ground). In addition, the impact of the model order was also investigated, e.g., when x(t) = $[\dot{z}_{psi}(t), \dot{z}_{psi}(t-1)].$

A same procedure was adopted for the GTR point. Throughout this work, \dot{z}_{psi} or \dot{z}_{gtr} is replaced by \dot{z} for simplicity (logically, the same applies to the dependent derivatives). The impact of each input variant as well as model order on the angle estimations will be discussed in detail in the Results section.

To train the network, for each participant, 25% of the data of each speed was used. The performance of the algorithm was then tested by the remaining 75% of the data of that participant for each of the eight speeds. This procedure was implemented for each of the joints under study. In the Results section, further discussion is provided about why this percentage was selected (Tab. 2).

D. PERFORMANCE MEASURES

To evaluate the quality of the estimations, the following three success measures were used:

- 1) The root mean square (RMS) errors $(\sqrt{\frac{\sum_{j=1}^{k}(\theta_{j}-\hat{\theta}_{j})^{2}}{k}})$,
- 2) the mean absolute errors (MAEs, $\frac{\sum_{j=1}^{k} |\theta_j \hat{\theta}_j|}{k}$), and 3) correlation coefficient ($\rho_{cc} = \frac{\sum_{j=1}^{k} (\theta_j \bar{\theta})(\hat{\theta}_j \bar{\theta})}{\sqrt{\sum_{j=1}^{k} (\theta_j \bar{\theta})^2} \sqrt{\sum_{j=1}^{k} (\hat{\theta}_j \bar{\theta})^2}}$),

[7], [8], [59], where k is the number of the variables, and $\hat{\theta}$ and θ are the estimated and actual joint positions (ankle, knee, hip), respectively. In the following section, the results of the previously discussed case studies are reported.

III. RESULTS AND DISCUSSIONS

Tab. 1, is a comprehensive table that compares the performance of the estimator with respect to different input variants and model orders. In addition, it compares the performance with regard to using PSI vs. GTR points. The estimation results using PSI and GTR points are denoted by θ_r^P , and θ_r^G , respectively, where x refers to hip h, knee k, or ankle a.

As seen in Tab. 1, six main case studies are developed. The results are for the following input cases, 1) x(t) = $[\dot{z}(t)], \ 2) \ x(t) = [\dot{z}(t), \dot{z}(t-1)], \ 3) \ x(t) = [\ddot{z}(t)], \ 4)$ $x(t) = [\ddot{z}(t), \ddot{z}(t-1)], 5) x(t) = [\dot{z}(t), \ddot{z}(t)], \text{ and } 6) x(t) =$ $[\dot{z}(t), \dot{z}(t-1), \ddot{z}(t), \ddot{z}(t-1)]$. In each case, those three joint angles are estimated once using PSI, and next using GTR points, separately. In the left half of Tab. 1, the results are reported for the first order models, and in the right half, the results of the second order models are brought. Furthermore, the results can be compared based on using the velocities, or accelerations, or combined inputs.

Fig. 3 comparatively shows RMS errors, MAEs, and ρ_{cc} values in one place for all three joints, and all case studies reported in Tab. 1. Each column of the figure is related to one case study mentioned previously in Tab. 1, which contains



TABLE 1. Comparison of average RMS errors [°], Mean Absolute Errors (MAEs) [°], and correlation coefficients ρ_{cc} according to input variants and model order (Estim. *using* PSI^P or GTR^G).

	RMSE MAE $ ho_{cc}$	RMSE MAE ρ_{cc}
$\frac{\text{inputs} \rightarrow}{\text{outputs} \downarrow}$	$x(t) = [\dot{z}(t)]$	$x(t) = [\dot{z}(t), \dot{z}(t-1)]$
$rac{ heta_h^P}{ heta_h^G}$	8.2±1.6 6.9±1.4 0.81±0.08 8.7±1.7 7.4±1.5 0.78±0.08	5.1±1.9 3.9±1.5 0.93±0.07 4.0±1.6 3.1±1.1 0.96±0.05
$rac{ heta_k^P}{ heta_k^G}$	17.5±1.7 14.2±1.4 0.41±0.05 17.4±1.5 14.2±1.3 0.41±0.06	$8.0\pm2.6 \mid 5.6\pm1.8 \mid 0.90\pm0.07$ $6.4\pm1.8 \mid 4.5\pm1.3 \mid 0.94\pm0.03$
$ heta_a^P \ heta_a^G$	6.8±1.3 5.3±0.9 0.33±0.13 6.6±1.2 5.2±0.9 0.39±0.10	$3.7 \pm 0.9 \mid 2.7 \pm 0.6 \mid 0.85 \pm 0.07$ $3.4 \pm 0.7 \mid 2.4 \pm 0.4 \mid 0.88 \pm 0.05$
	$x(t) = [\ddot{z}(t)]$	$x(t) = [\ddot{z}(t), \ddot{z}(t-1)]$
$rac{ heta_h^P}{ heta_h^G}$	12.7±1.6 11.0±1.5 0.39±0.17 12.0±1.4 10.3±1.3 0.49±0.14	5.4±1.8 4.1±1.3 0.92±0.06 4.1±1.4 3.2±1.0 0.96±0.05
$rac{ heta_k^P}{ heta_k^G}$	$\begin{array}{c c} 11.6 \pm 1.8 & 8.7 \pm 1.5 & 0.79 \pm 0.07 \\ 11.3 \pm 2.2 & 8.6 \pm 1.8 & 0.80 \pm 0.09 \end{array}$	$8.4\pm2.3 \mid 6.0\pm1.7 \mid 0.89\pm0.06 6.9\pm2.0 \mid 4.8\pm1.4 \mid 0.93\pm0.04$
$ heta_a^P \ heta_a^G$	5.5±1.1 4.4±0.9 0.63±0.13 5.0±1.2 4.0±1.0 0.70±0.10	$3.8\pm0.8 \mid 2.8\pm0.6 \mid 0.84\pm0.07$ $3.3\pm0.6 \mid 2.4\pm0.4 \mid 0.89\pm0.03$
	$x(t) = [\dot{z}(t), \ddot{z}(t)]$	$x(t) = [\dot{z}(t), \dot{z}(t-1), \ddot{z}(t), \ddot{z}(t-1)]$
$rac{ heta_h^P}{ heta_h^G}$	5.2±1.9 4.0±1.4 0.92±0.07 4.3±1.5 3.3±1.0 0.95±0.05	$4.5\pm1.8 \mid 3.5\pm1.3 \mid 0.95\pm0.07$ $3.5\pm1.4 \mid 2.7\pm0.9 \mid 0.97\pm0.05$
$rac{ heta_k^P}{ heta_k^G}$	$7.9\pm2.4 \mid 5.6\pm1.8 \mid 0.91\pm0.06 6.0\pm1.8 \mid 4.3\pm1.2 \mid 0.95\pm0.04$	$6.7 \pm 2.2 \mid 4.9 \pm 1.6 \mid 0.93 \pm 0.05 5.8 \pm 1.7 \mid 4.1 \pm 1.2 \mid 0.95 \pm 0.03$
$ heta_a^P \ heta_a^G$	$3.8\pm0.9 \mid 2.8\pm0.6 \mid 0.84\pm0.07 3.3\pm0.8 \mid 2.4\pm0.5 \mid 0.89\pm0.05$	3.5±0.8 2.5±0.5 0.87±0.05 3.0±0.5 2.2±0.4 0.91±0.03

results both for PSI (red circles) and GTR (Blue circles) points. The results are for forty-two participants, and the squares show the mean values in each case. For each case, the mean values show the average of all of the subjects and all of the speeds. Furthermore, Fig. 4 shows the results for three of the participants where actual and estimated hip joint positions are compared.

Logically, an estimator with fewer number of components in x(t) would be more desirable as it lessens the computational efforts. However, looking at Tab. 1 and Fig. 3 shows that using $x(t) = [\dot{z}(t)]$ or $x(t) = [\ddot{z}(t)]$ led to the lowest performance in comparison to the remaining four cases (both for PSI and GTR points). For the hip joint, the performance of $x(t) = [\dot{z}(t)]$ is better than $x(t) = [\ddot{z}(t)]$, however for ankle and knee it was the opposite.

It is observed that when model order is increased from $x(t) = [\dot{z}(t)]$ to $x(t) = [\dot{z}(t), \dot{z}(t-1)]$, the differences between the results get very obvious. For instance, for the ankle joint, the average ρ_{cc} increased nearly 157%, and 125%, for PSI and GTR points, respectively. For the knee joint, the corresponding value increases 119% and 129%, respectively. For the hip joint, the average ρ_{cc} increases less in comparison

to knee and ankle joints, about 14% and 23%, for PSI and GTR points, respectively.

A similar result is seen when model order is increased from $x(t) = [\ddot{z}(t)]$ to $x(t) = [\ddot{z}(t), \ddot{z}(t-1)]$. However, this time, the differences between the results for the hip joint are more obvious. In this case, the average ρ_{cc} increases nearly 135%, and 95%, for PSI and GTR points, respectively.

Not *very* noticeable differences between the results of $x(t) = [\dot{z}(t), \ddot{z}(t)]$ and $x(t) = [\dot{z}(t), \dot{z}(t-1), \ddot{z}(t), \ddot{z}(t-1)]$ are observed. Although, the former is a first order model in comparison to the latter which is a second order one. For instance, for the hip joint, the average ρ_{cc} increases nearly 3%, and 2%, for PSI and GTR points, respectively. Having in mind the previous paragraphs, one can conclude that the number of the inputs (in this case two inputs in $x(t) = [\dot{z}(t), \ddot{z}(t)]$) was also an important factor, when comparing the results with $x(t) = [\dot{z}(t)]$ or $x(t) = [\ddot{z}(t)]$.

With increasing the model order to 2 (right half of Tab. 1), the difference between $x(t) = [\dot{z}(t), \dot{z}(t-1)]$ and $x(t) = [\ddot{z}(t), \ddot{z}(t-1)]$ is relatively negligible. This trend is observed for both PSI and GTR points. However, for both inputs, the results related to GTR are better than PSI. Furthermore, the



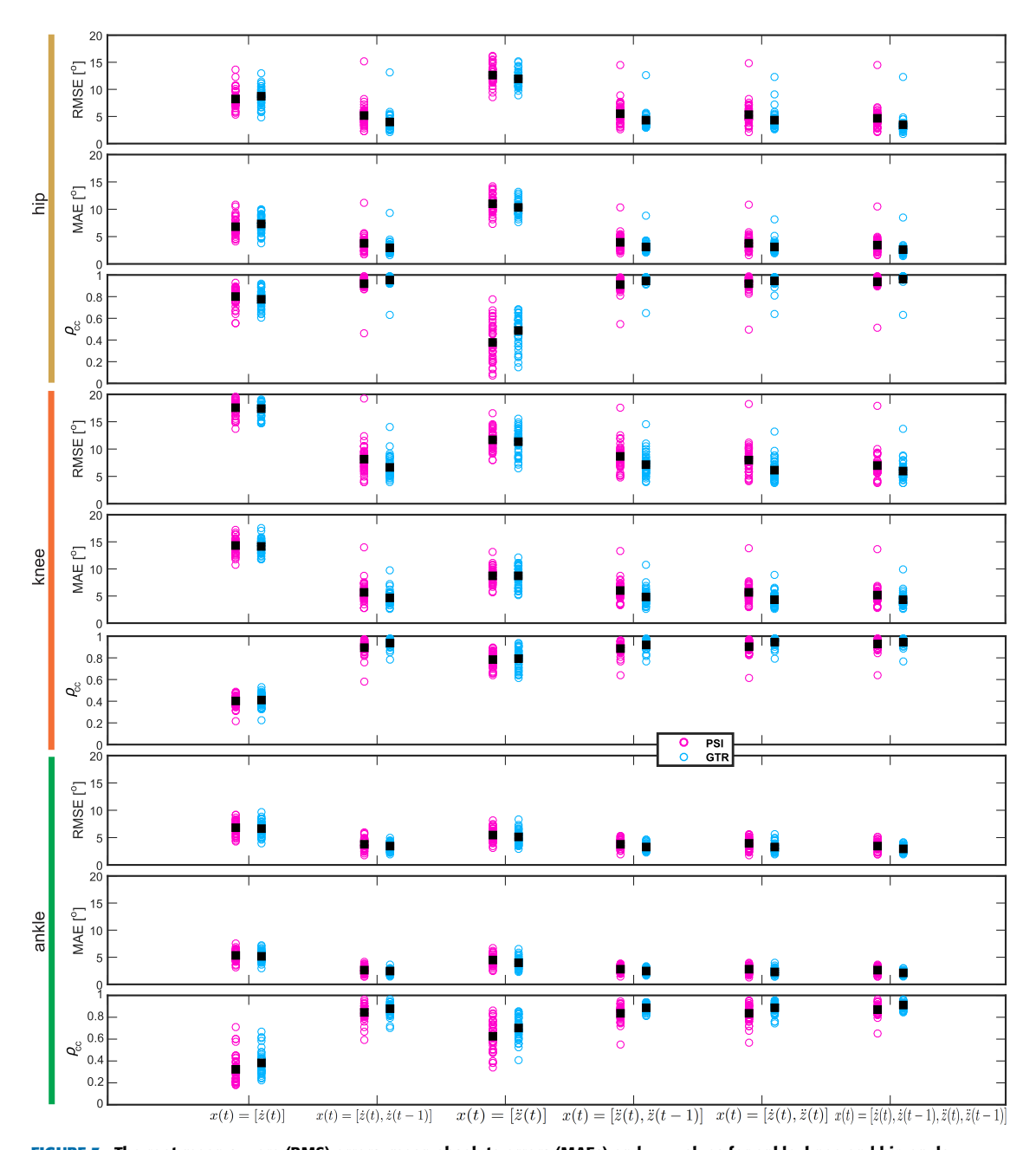


FIGURE 3. The root mean square (RMS) errors, mean absolute errors (MAEs) and ρ_{CC} values for ankle, knee and hip angle estimations according to different case studies explained in the Methods and Results section. Blue circles are related to the estimations using GTR point, and the red circles refer to the PSI point. Black squares show the mean of all of the subjects and all of the speeds for each case study.

results of these two cases are relatively similar to $x(t) = [\dot{z}(t), \ddot{z}(t)]$. Tab. 1 and Fig. 3 show that the best performance is observed when $x(t) = [\dot{z}(t), \dot{z}(t-1), \ddot{z}(t), \ddot{z}(t-1)]$. For these two latter cases, again it is observed that the estimations have higher accuracy using GTR point.

According to Tab. 1 and Fig. 3, the best ρ_{cc} results are seen for the hip angle estimation. The lowest performance is observed for the ankle angle estimation. Interestingly, this is regardless of the input variant (excluding $x(t) = [\ddot{z}(t)]$).

The above findings can create a guideline for motion planning and high-level controlling of active orthotics, prosthetics, or exoskeletons. The control design can start at first with less complex inputs such as $x(t) = [\dot{z}(t), \dot{z}(t-1)]$, $x(t) = [\ddot{z}(t), \ddot{z}(t-1)]$, or $x(t) = [\dot{z}(t), \ddot{z}(t)]$. Next, the results can be compared with those of a more complex input such as $x(t) = [\dot{z}(t), \dot{z}(t-1), \ddot{z}(t), \ddot{z}(t-1)]$. If the impact is slight, it may be safe to employ the less-inputs scenario. In addition, the designer may prefer only one type of the input, i.e., only velocity or only acceleration; both of which had more acceptable performance using a second-order model.

In general, different combinations of variables in x(t) are possible, e.g., $x(t) = [\dot{z}(t), \dot{z}(t-1), \dot{z}(t-2)]$ or x(t) =

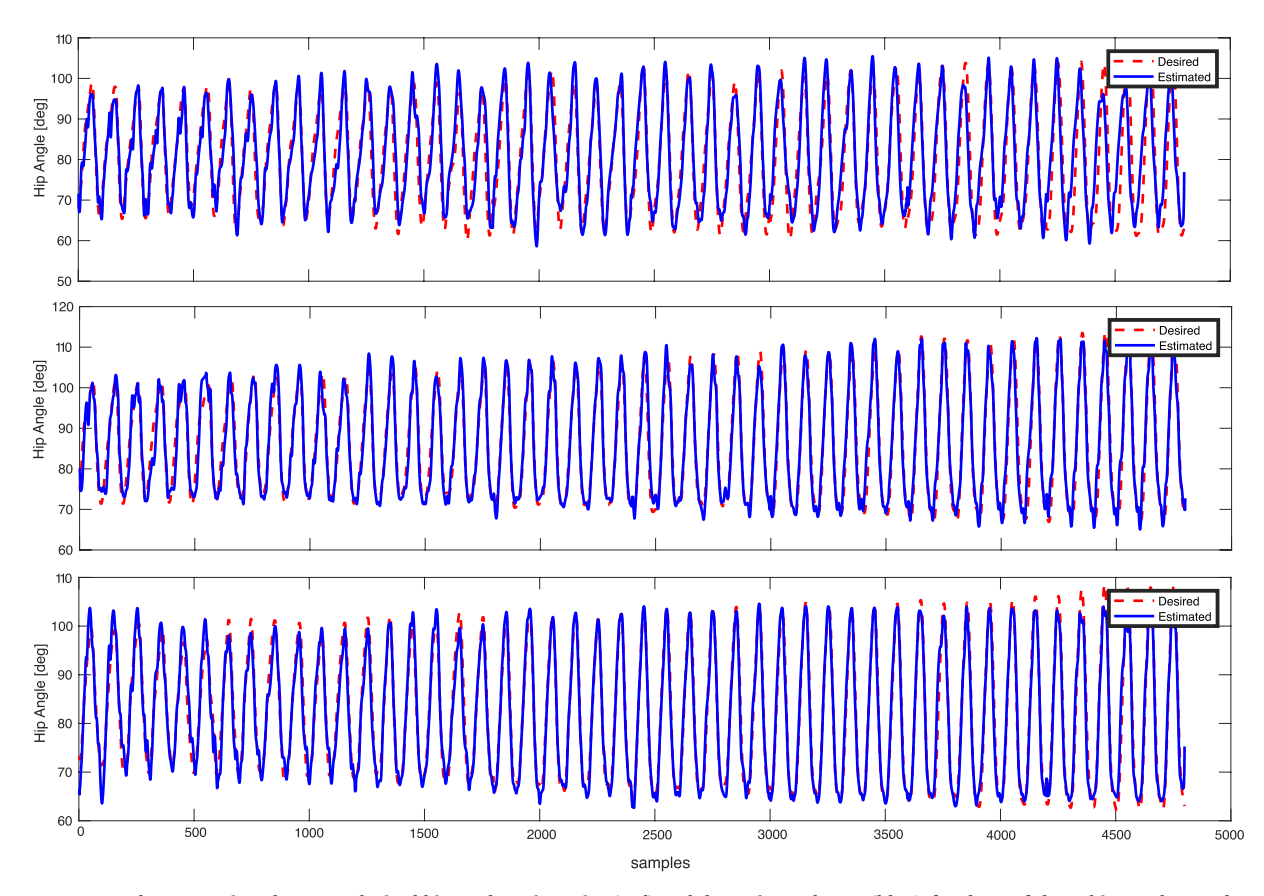


FIGURE 4. The comparison between desired hip angle trajectories (red) and the estimated ones (blue), for three of the subjects. The results are for estimations based on PSI and when $x(t) = [\dot{z}(t), \dot{z}(t-1), \ddot{z}(t), \dot{z}(t-1)]$.

TABLE 2. Comparison of average RMS errors [°], MAEs [°], and ρ_{cc} when different percentages of data was used for training.

	RMSE	MAE	$ ho_{cc}$	Percentage
$\frac{\text{inputs} \rightarrow}{\text{outputs} \downarrow}$	x(t) =	$[\dot{z}(t),\dot{z}(t-$	1)]	
θ_h^P	5.4±2.2 4.	1±1.7 0.9	92±0.10	12%
$ heta_h^P$	5.1±1.9 3.	9±1.5 0.9	93 ± 0.07	25%
$ heta_h^P$	4.9±1.5 3.	8±1.1 0.9	94 ± 0.05	35%
$ heta_h^P$	4.8±1.4 3.	8±1.2 0.9	94 ± 0.04	50%
$ heta_h^P$	4.9±1.4 3.	$8\pm1.2 \mid 0.9$	94 ± 0.05	75%
$ heta_h^P$	4.9±1.5 3.	$9\pm1.3 \mid 0.9$	93 ± 0.05	85%

 $[\dot{z}(t-1),\dot{z}(t-2)]$, etc. While this will be interesting, it was out of the scope of this work to evaluate exhaustively so many possibilities and combinations that exist and may come to mind, some of which, may have similar results. Here, the results for one example are presented when $x(t) = [\dot{z}(t),\dot{z}(t-1),\dot{z}(t-2)]$, using GTR point. For hip angles estimation, the average RMS error [°], MAE [°] and ρ_{cc} , were 4.0 ± 1.6 , 3.0 ± 1.1 and 0.96 ± 0.05 , respectively. For knee joint, the average values are 6.2 ± 1.8 , 4.4 ± 1.3 , and 0.94 ± 0.03 . For ankle joint, the average values are 3.3 ± 0.7 , 2.4 ± 0.5 , 0.88 ± 0.05 , respectively.

TABLE 3. Comparison of average RMS errors [°], MAEs [°], and $\rho_{\rm CC}$ when sigmoid function estimator was used for estimation.

	RMSE MAE $ ho_{cc}$
$\frac{\text{inputs} \rightarrow}{\text{outputs} \downarrow}$	$x(t) = [\dot{z}(t), \dot{z}(t-1)]$
$ heta_h^P$	$6.4{\pm}1.4 \mid 5.1{\pm}1.2 \mid 0.89{\pm}0.06$
$ heta_h^G$	$5.5{\pm}1.3 \mid 4.3{\pm}1.0 \mid 0.92{\pm}0.05$
$ heta_k^P$	$11.9 \pm 2.2 \mid 8.9 \pm 1.9 \mid 0.78 \pm 0.08$
$ heta_k^G$	$9.1{\pm}2.2 \mid 6.6{\pm}1.6 \mid 0.88{\pm}0.06$
$ heta_a^P$	$5.0\pm0.9 \mid 3.6\pm0.6 \mid 0.72\pm0.07$
$ heta_a^G$	$4.8{\pm}0.8 \mid 3.6{\pm}0.5 \mid 0.74{\pm}0.06$
	$x(t) = [\ddot{z}(t), \ddot{z}(t-1)]$
$ heta_h^P$	$6.4{\pm}1.6 \mid 5.1{\pm}1.2 \mid 0.90{\pm}0.06$
$ heta_h^G$	$4.8 \pm 1.5 \mid 3.8 \pm 1.1 \mid 0.94 \pm 0.05$
$ heta_k^P$	$10.4\pm2.0 \mid 7.4\pm1.5 \mid 0.84\pm0.06$
$ heta_k^G$	$9.1{\pm}2.0 \mid 6.4{\pm}1.6 \mid 0.88{\pm}0.06$
θ_a^P	$5.0\pm1.0 \mid 3.7\pm0.7 \mid 0.73\pm0.07$
θ_a^G	$4.7\pm1.2 \mid 3.3\pm0.6 \mid 0.77\pm0.09$
	<u> </u>

As observed, increasing the dimension of the input x(t) does not necessarily improve the results (or very slightly in some cases) in comparison to the results seen in Tab. 1, for



 $x(t) = [\dot{z}(t), \dot{z}(t-1)]$ in the top right column. This can be an important point that can lead to less computational efforts.

For the estimations, it is aimed to avoid using the previous output estimation into the input structure. Further investigations shows that its inclusion could even worsen the performance. For instance, for the hip angle estimation, when $x(t) = [\hat{y}(t-1), \dot{z}(t)], \ \rho_{cc}$ reduces to 0.08 ± 0.14 (GTR). In addition, not using the previous outputs decouples the performance of the estimator from the output, and makes it a function of only the inputs that originate from PSI or GTR points. In addition, it can lead to less computational load for the high-level controller.

It was mentioned in Methods section that 25% of the data was used for training. Table 2, shows the results of estimations when different portions of the data was used for training. The table shows the results for $x(t) = [\dot{z}(t), \dot{z}(t-1)]$, when PSI was used to estimate hip joint positions. Comparing the results shows that the best performance is seen between 35% - 75%, although in comparison to the portion selected for this study (i.e., the second row), the differences are not very considerable. For the case of using 25% of data, the average ρ_{cc} decreased about 1% in comparison to using 50% of data. The table provides some insights about the importance of reaching a balanced compromise between the training effort and the results quality. The table also shows that when 85% of the data was used, the results declined again.

As mentioned previously in the Methods section, different estimator functions can be used for estimations. The results were shown and discussed for the wavelet-based estimator function. In addition to that, the impact of another estimator function is also investigated. In one case study, sigmoid function is used to estimate the output signals. Table 3 compares the ankle, knee and hip angle estimations when PSI and GTR points are used for estimation, for the cases $x(t) = [\dot{z}(t), \dot{z}(t-1)]$ and $x(t) = [\ddot{z}(t), \ddot{z}(t-1)]$. The table shows that the results are less accurate than the ones observed in Tab. 1 for the corresponding case studies. In addition, the results related to GTR point have higher accuracy again, similar to what was observed in Tab. 1. Future investigations can better reveal the full potential of each candidate for the estimator function.

IV. FURTHER DISCUSSIONS AND CONCLUSION

In this study, it was suggested to use the motion of the GTR or PSI (separately) as candidate input points, to estimate leg joints' positions during walking.

The outcomes of this study can be used in different applications, e.g., in case of a hip orthosis, a full-leg orthosis, power-augmentation exoskeletons, or prosthetics. As it was mentioned in Introduction, the viewpoint of this study had a fundamental difference with several studies related to the angle/moment estimations. It was discussed that obtaining information from a point which is hierarchically lower than the joint under investigation, could potentially lead to a paradoxical situation for the high-level controller.

In case of a hip orthosis, the motion of the PSI/GTR would be influenced (controlled) by both central nervous system and the operation of the hip orthosis, whereas the motion of the thigh would be mainly directly influenced by the orthotic device. Because of this difference, for the above case, it may be logical to think that the inputs originating from the PSI/GTR can be more reliable than the inputs coming directly from the thigh. This might potentially lead to a more robust controller at the end. Other than paying attention to the natural hierarchy in human body, the other point that was paid attention was the usability of the developed method in the context of orthotics/prosthetics. As an example, stride length, cadence, and the lengths of leg limbs were used to estimate leg joints' position [9]. This approach can potentially have two issues if one wants to use for the prosthesis control. First, the stride length and cadence are *direct* outcomes of the performance of the prosthetic device and using them for intent recognition could be controversial. The second is that the proposed method used biological limbs' lengths, which for amputees can be unobtainable. Lots of studies can be found which lie in this category, e.g., [18], [21], [60], [61].

There are fewer studies which have attitude similar to the one presented in this study when estimating the positions of a specific joint for orthotic/prosthetic applications. Rectus femoris and semitendinosus EMG sgmals were used to estimate knee positions in [14]. Four subjects were asked to walk at a self-selected speed. The average results of ρ_{cc} were between 0.59±0.90 and 0.84±0.07. Tibialis anterior and gastrocnemius EMG signals were used to estimate ankle joint positions in [62]. The authors used a dataset which involved data for a wide age range (from 6-72 yrs old). The subjects were asked to walk at four different speeds, very slow, slow, medium, and fast, according to their height. The RMS error, and ρ_{cc} for the ankle joint positions were 2.4°±0.15°, and 0.95, respectively (no further information was found for st.d. of ρ_{cc} , in addition no information was found for MAEs). Displacement, linear velocity, and acceleration (in xy directions, obtained form a sacrum-attached IMU), together with time was used to estimate hip, knee, and ankle angles in [39]. Seven subjects were asked to walk on a treadmill. The average speeds were 1.3 m/s (slow), 1.4 m/s (moderate), and 1.8 m/s (fast). They proposed to use feed-forward neural network to estimate joint positions in stance phase. The RMS errors were $3.14^{\circ}\pm1.49^{\circ}$, $2.17^{\circ}\pm1.23^{\circ}$, and $3.35^{\circ}\pm1.58^{\circ}$, for hip, knee, and ankle joints, respectively. The values of ρ_{cc} were 0.99 \pm 0.03, 0.99 \pm 0.00, 0.99 \pm 0.01, for hip, knee, and ankle joints, respectively. Similar to [3], phase plane concept was used to estimate hip, knee and ankle positions in [5]. The inputs to the model were thigh angle and its integral, as well as a rule to reset the integral at the start of each stride. To estimate joint angles, the algorithm required to determine the gait percent and type of the locomotion. To do this, basis functions were developed for phase estimation, and task functions were defined to take into account the type of gaits. Similar study was conducted by the authors in [40]. The RMS errors were



TABLE 4. Comparison of this study with different studies (see also section IV for more information).

Study & Joints	Quantity of Sources & Type of the Inputs	Estimation Algorithm	No. of Participants	Speeds	Ave. RMSE [°]	Ave. MAE [°]	Ave. $ ho_{cc}$
[7] (Hip) [7] (Kne) [7] (Ank.)	3 foot ang. vel. & lin. acc.	GRNN	8	moderate	2.4 – 2.7 2.8 4.7 – 5.3	1.7 - 1.9 1.8 $3.3 - 3.7$	0.99 0.99 0.98 – 0.99
[8] (Kne.)	12 3D ang. vel. & lin. acc.	GRNN	8	moderate	_	7.1 – 7.6	0.88 - 0.89
[8] (Ank.)	from shank & foot	OIG 111		moderate		4.9 - 5.3	0.70 - 0.75
[63] (Kne.)	12 3D ang. vel. & acc. from thigh & shank	Rotation Matrices	3	moderate	6.8	4.6	0.92
[14] (Kne.)	2 EMG signals	MLP NN	4	moderate	_	_	0.59 - 0.84
[9] (Kne.)	6 stride length,	DFT	70	slow &		5.4	0.97
[9] (Ank.)	cadence, etc.	& GRNN	70	moderate	-	3.6	0.92
[60] (Kne.)	14 height, mass,	GPR	113	moderate	_	6.95 – 7.05	
[60] (Ank.)	gender, etc.	OI K	115	moderate		4.20 - 4.29	
[18] (Kne.)	10 EMG signals	deep belief NN	6	0.8, 1, 1.2 m/s	3.9	_	0.97
[18] (Ank.)	10 Livio signais	deep benef 1414	0	0.0, 1, 1.2 11//3	2.4		0.95
[16] (Ank.)	3 EMG signal	NARX Net (without wavelets)	3	moderate	1.2 – 5.4	_	_
[61] (Ank.)	9 gait events	feedforward NN	10	moderate	1.2 – 2		
[21] (Ank.)	4 EMG & kinema.	NARX Net (without wavelets)	10	moderate	2.4	_	0.97
[62] (Ank.)	3 EMG signals	feedforward NN	40	very slow to fast	1.1 – 2.3	_	0.96 – 0.99
[39] (Hip)	7 6	FF NN	7	1.2, 1.4, 1.8	3.1	_	0.99
(Kne.)	7 Sacrum acc., vel., displa., time				2.1	_	0.99
(Ank.)	displa., time				3.3	_	0.99
[23] (Kne.)	$7 \mid ext{EMG}, heta_{th}, \dot{ heta}_{th} \ heta_{sh}, \dot{ heta}_{sh}$	deep-recurrent NN	11	moderate	2.9	_	_
[40] (Hip) [5] (Kne.)	$2^+ \mid \theta_{th}, \int \theta_{th}, \&$ integral reset	DFT & weighted task inclusion	10	0.8, 1, 1.2	2.5 [40] 4.1 [40]	_	_
[5] (Ank.)					3.4 [40]	_	
[29] (Hip) [29] (Kne.) [29] (Ank.)	12 lin. acc.& ang. vel. (waist, shank, thigh)	deep learning with convolu. & recurr. layers	27	1.1 – 3.8	— —	3.2-4.1 2.6-3.7 4.5-5.9	0.99 0.99 0.95 – 0.98
[11] (Kne.)	$2 \mid \theta_{th}, \dot{\theta}_{th}$	GPR	23	0.5, 1, 1.5	4.4 – 6.2	3.3 – 4.4	0.55 - 0.56
[10] (Ank.)	$\frac{2 \mid \theta_{th}, \theta_{th}}{2 \mid \theta_{sh}, \dot{\theta}_{sh}}$	GPR	23	0.5, 1, 1.5	2.1 – 2.3	3.3 – 4.4	
	$2 \mid \sigma_{sh}, \sigma_{sh}$	Urk	21	0.5, 1, 1.5			0.07
This study θ_h^G θ_k^G θ_a^G	2 ż, ż 2 ż, ż 2 ż, ż 2 ż, ż	wavelets & NARX	42	8 different speeds 0.4 - 2.2 m/s	3.5 5.8 3.0	2.7 4.1 2.2	0.97 0.95 0.91

GRNN: Generalized Regression Neural Network

DFT: Discrete Fourier Transform

 $3.48^{\circ}\pm0.60^{\circ}$, $4.14^{\circ}\pm0.92^{\circ}$, $2.53^{\circ}\pm0.81^{\circ}$, for ankle, knee and hip joints, respectively (for ten subjects walking at 0.8, 1.0, and 1.2 m/s). Table 4 provides a comprehensive information regarding the outcomes of several studies. In addition, one can compare the results of different performance measures and different studies as well as this study at the same time.

As can be observed from Tab. 4, the values obtained in this study are also within the range of the values reported by the above studies. One point to pay attention here is that, for instance, the method presented e.g., in [40] or in [7] is not applicable in case of a hip orthosis (due to hierarchy reasons that were previously discussed in this work), or the method presented by [62] was only related to the ankle joint. Some studied also used more inputs than our proposed approach, e.g., [39].

For the control purpose, an IMU can be attached to the PSI/GTR points which can act as the input source. The GTR IMU can be attached around the axis of rotation of the hip joint in a hip orthosis. For the PSI point, in real-world applications, a customized belt can be worn by the user. In case of a full-leg orthosis, or power-augmentation exoskeleton, the IMU can be already directly attached to the device around the waist area. Using IMUs near to this point was already investigated e.g., in [29] and [39] (see also Tab. 4).

The method presented in this study, estimated the whole leg joints' positions. Therefore, it can be used in motion planning and high-level controlling of humanoids, exoskeletons, orthotics, and prosthetics, whose actuation mechanisms do not have an elastic component such as a spring, e.g, [4], [64], [65], or [66] (knee joint). In this situation, the joint



trajectory (trend) would be similar to that of the actuator and can be mapped accordingly, taking into account the ratios related to the intermediate transmissions, if any. in addition, the results showed that the proposed method can be used for subjects at different ages as in this study data-set of participants with a very wide age range was used. Although using data from very diverse population could reduce the quality of the outputs, looking at the results showed that the estimator behaved relatively robustly against this (possibly disruptive) factor.

In this study, the algorithm was tested for walking gait. Furthermore, in this study the joints' motions were analyzed in the sagittal plane, where relatively large range-of-motion happens. One direction for future works can be to analyze the quality of the estimations for other anatomical planes such as frontal and/or transverse planes. Future works can also involve investigating the performance of the proposed estimation algorithm for other gaits such as ascending and descending the stairs and/or slopes, and running. Furthermore, it can also be investigated if using both points simultaneously, can increase the efficiency of the algorithm. In addition, another direction for future investigations can be to determine the most optimal components as well as dimension of the input matrix.

ACKNOWLEDGMENT

The authors would like to express their gratitude to the authors of [47] for making their data publicly available.

REFERENCES

- [1] D. L. Grimes, W. C. Flowers, and M. Donath, "Feasibility of an active control scheme for above knee prostheses," *J. Biomechanical Eng.*, vol. 99, no. 4, pp. 215–221, Nov. 1977.
- [2] H. Vallery, E. H. F. van Asseldonk, M. Buss, and H. van der Kooij, "Reference trajectory generation for rehabilitation robots: Complementary limb motion estimation," *IEEE Trans. Neural Syst. Rehabil. Eng.*, vol. 17, no. 1, pp. 23–30, Feb. 2009.
- [3] M. A. Holgate, T. G. Sugar, and A. W. Bohler, "A novel control algorithm for wearable robotics using phase plane invariants," in *Proc. IEEE Int. Conf. Robot. Autom.*, May 2009, pp. 3845–3850.
- [4] D. Quintero, D. J. Villarreal, D. J. Lambert, S. Kapp, and R. D. Gregg, "Continuous-phase control of a powered Knee–Ankle prosthesis: Amputee experiments across speeds and inclines," *IEEE Trans. Robot.*, vol. 34, no. 3, pp. 686–701, Jun. 2018.
- [5] K. R. Embry, D. J. Villarreal, R. L. Macaluso, and R. D. Gregg, "Modeling the kinematics of human locomotion over continuously varying speeds and inclines," *IEEE Trans. Neural Syst. Rehabil. Eng.*, vol. 26, no. 12, pp. 2342–2350, Dec. 2018.
- [6] K. R. Embry and R. D. Gregg, "Analysis of continuously varying kinematics for prosthetic leg control applications," *IEEE Trans. Neural* Syst. Rehabil. Eng., vol. 29, pp. 262–272, 2021.
- [7] J. Y. Goulermas, D. Howard, C. J. Nester, R. K. Jones, and L. Ren, "Regression techniques for the prediction of lower limb kinematics," *J. Biomechanical Eng.*, vol. 127, no. 6, pp. 1020–1024, Nov. 2005.
- [8] A. Findlow, J. Y. Goulermas, C. Nester, D. Howard, and L. P. J. Kenney, "Predicting lower limb joint kinematics using wearable motion sensors," *Gait Posture*, vol. 28, no. 1, pp. 120–126, Jul. 2008.
- [9] T. P. Luu, K. H. Low, X. Qu, H. B. Lim, and K. H. Hoon, "An individual-specific gait pattern prediction model based on generalized regression neural networks," *Gait Posture*, vol. 39, no. 1, pp. 443–448, Jan. 2014.
- [10] M. Eslamy and K. Alipour, "Synergy-based Gaussian process estimation of ankle angle and torque: Conceptualization for high level controlling of active robotic foot prostheses/orthoses," *J. Biomechanical Eng.*, vol. 141, no. 2, Feb. 2019, Art. no. 021002.

- [11] M. Eslamy, F. Oswald, and A. F. Schilling, "Estimation of Knee angles based on thigh motion: A functional approach and implications for high-level controlling of active prosthetic knees," *IEEE Control Syst. Mag.*, vol. 40, no. 3, pp. 49–61, Jun. 2020.
- [12] M. Eslamy, F. Oswald, and A. Schilling, "Mapping thigh motion to knee motion: Implications for motion planning of active prosthetic knees," in *Proc. IEEE/RSJ Int. Conf. Intell. Robots Syst. (IROS)*, Oct. 2020, pp. 4120–4125.
- [13] M. Eslamy and A. F. Schilling, "Estimation of knee and ankle angles during walking using thigh and shank angles," *Bioinspiration Biomimetics*, vol. 16, no. 6, Nov. 2021, Art. no. 066012.
- [14] A. L. Delis, J. L. A. Carvalho, A. F. da Rocha, R. U. Ferreira, S. S. Rodrigues, and G. A. Borges, "Estimation of the knee joint angle from surface electromyographic signals for active control of leg prostheses," *Physiolog. Meas.*, vol. 30, no. 9, pp. 931–946, Sep. 2009.
- [15] S. K. Au, P. Bonato, and H. Herr, "An EMG-position controlled system for an active ankle-foot prosthesis: An initial experimental study," in *Proc.* 9th Int. Conf. Rehabil. Robot. (ICORR), Aug. 2005, pp. 375–379.
- [16] S. Farmer, B. Silver-Thorn, P. Voglewede, and S. A. Beardsley, "Within-socket myoelectric prediction of continuous ankle kinematics for control of a powered transtibial prosthesis," *J. Neural Eng.*, vol. 11, no. 5, Oct. 2014, Art. no. 056027.
- [17] U. Mamikoglu, G. Andrikopoulos, G. Nikolakopoulos, U. Röijezon, M. Pauelsen, and T. Gustafsson, "Electromyography based joint angle estimation and control of a robotic leg," in *Proc. 6th IEEE Int. Conf. Biomed. Robot. Biomechatronics (BioRob)*, Jun. 2016, pp. 182–187.
- [18] J. Chen, X. Zhang, Y. Cheng, and N. Xi, "Surface EMG based continuous estimation of human lower limb joint angles by using deep belief networks," *Biomed. Signal Process. Control*, vol. 40, pp. 335–342, Feb. 2018.
- [19] I. Jolliffe, Principal Component Analysis, 2nd ed. New York, NY, USA: Springer-Verlag, 2002.
- [20] H. Huang, F. Zhang, L. J. Hargrove, Z. Dou, D. R. Rogers, and K. B. Englehart, "Continuous locomotion-mode identification for prosthetic legs based on neuromuscular–mechanical fusion," *IEEE Trans. Biomed. Eng.*, vol. 58, no. 10, pp. 2867–2875, Oct. 2011.
- [21] R. Gupta, I. S. Dhindsa, and R. Agarwal, "Continuous angular position estimation of human ankle during unconstrained locomotion," *Biomed. Signal Process. Control*, vol. 60, Jul. 2020, Art. no. 101968.
- [22] A. J. Young, T. A. Kuiken, and L. J. Hargrove, "Analysis of using EMG and mechanical sensors to enhance intent recognition in powered lower limb prostheses," *J. Neural Eng.*, vol. 11, no. 5, Oct. 2014, Art. no. 056021.
- [23] Y. Huang, Z. He, Y. Liu, R. Yang, X. Zhang, G. Cheng, J. Yi, J. P. Ferreira, and T. Liu, "Real-time intended knee joint motion prediction by deep-recurrent neural networks," *IEEE Sensors J.*, vol. 19, no. 23, pp. 11503–11509, Dec. 2019.
- [24] I. Kang, P. Kunapuli, and A. J. Young, "Real-time neural network-based gait phase estimation using a robotic hip exoskeleton," *IEEE Trans. Med. Robot. Bionics*, vol. 2, no. 1, pp. 28–37, Feb. 2020.
- [25] C. B. Sanz-Morère, E. Martini, B. Meoni, G. Arnetoli, A. Giffone, S. Doronzio, C. Fanciullacci, A. Parri, R. Conti, F. Giovacchini, E. Frioriksson, D. Romo, S. Crea, R. Molino-Lova, and N. Vitiello, "Robot-mediated overground gait training for transfemoral amputees with a powered bilateral hip orthosis: A pilot study," *J. NeuroEng. Rehabil.*, vol. 18, no. 1, pp. 1–17, Dec. 2021.
- [26] S. Hood, L. Gabert, and T. Lenzi, "Powered knee and ankle prosthesis with adaptive control enables climbing stairs with different stair heights, cadences, and gait patterns," *IEEE Trans. Robot.*, vol. 38, no. 3, pp. 1430–1441, Jun. 2022.
- [27] F. Sup, A. Bohara, and M. Goldfarb, "Design and control of a powered transfemoral prosthesis," *Int. J. Robot. Res.*, vol. 27, no. 2, pp. 263–273, Feb. 2008.
- [28] Y. Guo, F. Storm, Y. Zhao, S. Billings, A. Pavic, C. Mazzà, and L.-Z. Guo, "A new proxy measurement algorithm with application to the estimation of vertical ground reaction forces using wearable sensors," *Sensors*, vol. 17, no. 10, p. 2181, Sep. 2017.
- [29] V. Hernandez, D. Dadkhah, V. Babakeshizadeh, and D. Kulić, "Lower body kinematics estimation from wearable sensors for walking and running: A deep learning approach," *Gait Posture*, vol. 83, pp. 185–193, Jan. 2021.
- [30] S. A. Gard, S. C. Miff, and A. D. Kuo, "Comparison of kinematic and kinetic methods for computing the vertical motion of the body center of mass during walking," *Human Movement Sci.*, vol. 22, no. 6, pp. 597–610, Apr. 2004.



- [31] G. A. Cavagna, "Force platforms as ergometers," J. Appl. Physiol., vol. 39, no. 1, pp. 174–179, Jul. 1975.
- [32] K. E. Gordon, D. P. Ferris, and A. D. Kuo, "Metabolic and mechanical energy costs of reducing vertical center of mass movement during gait," *Arch. Phys. Med. Rehabil.*, vol. 90, no. 1, pp. 136–144, 2009.
- [33] R. Staszkiewicz, T. Ruchlewicz, W. Forczek, and J. Laska, "The impact of changes in gait speed and step frequency on the extent of the center of mass displacements," *Acta Bioeng. Biomech.*, vol. 12, no. 3, pp. 13–20, 2010.
- [34] G. F. Devetak, R. C. D. Bohrer, A. L. F. Rodacki, and E. F. Manffra, "Center of mass in analysis of dynamic stability during gait following stroke: A systematic review," *Gait Posture*, vol. 72, pp. 154–166, Jul. 2019.
- [35] I. Kingma, H. M. Toussaint, D. A. C. M. Commissaris, M. J. M. Hoozemans, and M. J. Ober, "Optimizing the determination of the body center of mass," *J. Biomechanics*, vol. 28, no. 9, pp. 1137–1142, Sep. 1995.
- [36] H. Lim and S. Park, "Kinematics of lower limbs during walking are emulated by springy walking model with a compliantly connected, offcentered curvy foot," *J. Biomechanics*, vol. 71, pp. 119–126, Apr. 2018.
- [37] R. Blickhan, "The spring-mass model for running and hopping," J. Biomechanics, vol. 22, nos. 11–12, pp. 1217–1227, Jan. 1989.
- [38] H. Geyer, A. Seyfarth, and R. Blickhan, "Compliant leg behaviour explains basic dynamics of walking and running," *Proc. Roy. Soc. B, Biol. Sci.*, vol. 273, no. 1603, pp. 2861–2867, Nov. 2006.
- [39] H. Lim, B. Kim, and S. Park, "Prediction of lower limb kinetics and kinematics during walking by a single IMU on the lower back using machine learning," *Sensors*, vol. 20, no. 1, p. 130, Dec. 2019.
- [40] E. Reznick, K. Embry, and R. D. Gregg, "Predicting individualized joint kinematics over a continuous range of slopes and speeds," in *Proc. 8th IEEE RAS/EMBS Int. Conf. for Biomed. Robot. Biomechatronics (BioRob)*, Nov. 2020, pp. 666–672.
- [41] L. Ljung, System Identification, Theory for the User, 2nd ed. Upper Saddle River, NJ, USA: Prentice-Hall, 1999.
- [42] R. Isermann and M. Münchhof, *Identification of Dynamic Systems: An Introduction With Applications*. Cham, Switzerland: Springer, 2010.
- [43] I. Daubechies, "The wavelet transform, time-frequency localization and signal analysis," *IEEE Trans. Inf. Theory*, vol. 36, no. 5, pp. 961–1005, Sep. 1990.
- [44] S. G. Mallat, "A theory for multiresolution signal decomposition: The wavelet representation," *IEEE Trans. Pattern Anal. Mach. Intell.*, vol. 11, no. 7, pp. 674–693, Jul. 1989.
- [45] I. Daubechies, "Orthonormal bases of compactly supported wavelets," Commun. Pure Appl. Math., vol. 41, no. 7, pp. 909–996, Oct. 1988.
- [46] I. Daubechies Ten Lectures Wavelets. Philadelphia, PA, USA: SIAM, 1992.
- [47] C. A. Fukuchi, R. K. Fukuchi, and M. Duarte, "A public dataset of overground and treadmill walking kinematics and kinetics in healthy individuals," *PeerJ*, vol. 6, Apr. 2018, Art. no. e4640.
- [48] S. Lipfert, Kinematic and Dynamic Similarities Between Walking and Running. Hamburg, Germany: Verlag Dr. Kovac, 2010.
- [49] Q. Zhang, "Using wavelet network in nonparametric estimation," *IEEE Trans. Neural Netw.*, vol. 8, no. 2, pp. 227–236, Mar. 1997.
- [50] Q. Zhang and A. Benveniste, "Wavelet networks," *IEEE Trans. Neural Netw.*, vol. 3, no. 6, pp. 889–898, Nov. 1992.
- [51] A. A. Safavi and J. A. Romagnoli, "Comments on 'nonlinear black box modeling in system identification: A unified overview," *Automatica*, vol. 33, no. 6, pp. 1197–1198, Jun. 1997.
- [52] A. Juditsky, H. Hjalmarsson, A. Benveniste, B. Delyon, L. Ljung, J. SjÖberg, and Q. Zhang, "Nonlinear black-box models in system identification: Mathematical foundations," *Automatica*, vol. 31, no. 12, pp. 1725–1750, Dec. 1995.
- [53] T. Kugarajah and Q. Zhang, "Multidimensional wavelet frames," *IEEE Trans. Neural Netw.*, vol. 6, no. 6, pp. 1552–1556, Jan. 1995.
- [54] S. Chen, C. F. N. Cowan, and P. M. Grant, "Orthogonal least squares learning algorithm for radial basis function networks," *IEEE Trans. Neural Netw.*, vol. 2, no. 2, pp. 302–309, Mar. 1991.
- [55] D. Popovic and S. Jonic, "Determining synergy between joint angles during locomotion by radial basis function neural networks," in *Proc. 20th Annu. Int. Conf. IEEE Eng. Med. Biol. Soc. Biomed. Eng. Towards Year Beyond*, vol. 20, Nov. 1998, pp. 2301–2304.
- [56] S. Jonic, T. Jankovic, V. Gajic, and D. Popvic, "Three machine learning techniques for automatic determination of rules to control locomotion," *IEEE Trans. Biomed. Eng.*, vol. 46, no. 3, pp. 300–310, Mar. 1999.
- [57] I. Milovanovic, "Radial basis function (RBF) networks for improved gait analysis," in *Proc. 9th Symp. Neural Netw. Appl. Electr. Eng.*, Nov. 2008, pp. 129–132.

- [58] M. Thor, T. Kulvicius, and P. Manoonpong, "Generic neural locomotion control framework for legged robots," *IEEE Trans. Neural Netw. Learn.* Syst., vol. 32, no. 9, pp. 4013–4025, Sep. 2021.
- [59] R. A. Bogey and L. A. Barnes, "An EMG-to-force processing approach for estimating in vivo hip muscle forces in normal human walking," *IEEE Trans. Neural Syst. Rehabil. Eng.*, vol. 25, no. 8, pp. 1172–1179, Aug. 2017.
- [60] Y. Yun, H.-C. Kim, S. Y. Shin, J. Lee, A. D. Deshpande, and C. Kim, "Statistical method for prediction of gait kinematics with Gaussian process regression," *J. Biomechanics*, vol. 47, no. 1, pp. 186–192, Jan. 2014.
- [61] S. Sivakumar, A. A. Gopalai, K. H. Lim, and D. Gouwanda, "Artificial neural network based ankle joint angle estimation using instrumented foot insoles," *Biomed. Signal Process. Control*, vol. 54, Sep. 2019, Art. no. 101614.
- [62] A. D. Keleş and C. A. Yucesoy, "Development of a neural network based control algorithm for powered ankle prosthesis," *J. Biomechanics*, vol. 113, Dec. 2020, Art. no. 110087.
- [63] R. Takeda, S. Tadano, A. Natorigawa, M. Todoh, and S. Yoshinari, "Gait posture estimation using wearable acceleration and gyro sensors," *J. Biomechanics*, vol. 42, no. 15, pp. 2486–2494, Nov. 2009.
- [64] T. Elery, S. Rezazadeh, C. Nesler, and R. D. Gregg, "Design and validation of a powered Knee–Ankle prosthesis with high-torque, low-impedance actuators," *IEEE Trans. Robot.*, vol. 36, no. 6, pp. 1649–1668, Dec. 2020.
- [65] A. F. Azocar, L. M. Mooney, J.-F. Duval, A. M. Simon, L. J. Hargrove, and E. J. Rouse, "Design and clinical implementation of an open-source bionic leg," *Nature Biomed. Eng.*, vol. 4, no. 10, pp. 941–953, Oct. 2020.
- [66] F. Sup, H. A. Varol, J. Mitchell, T. Withrow, and M. Goldfarb, "Design and control of an active electrical knee and ankle prosthesis," in *Proc. 2nd IEEE RAS EMBS Int. Conf. Biomed. Robot. Biomechatronics*, Oct. 2008, pp. 523–528.



MAHDY ESLAMY received the bachelor's degree in mechanical engineering from IUST, Tehran, Iran, the master's degree in mechanical engineering from KNTU, Tehran, and the Ph.D. degree in mechanical engineering from the Technical University of Darmstadt, Germany. He is currently an Assistant Professor of mechanical engineering with Teesside University, U.K. He has passed two postdoctorals in Belgium and Germany. His main research and teaching expertise are in the fields

of design (dynamics/FEA), control, motion analysis, fluid mechanics, and biomechanics. He was a recipient of Iran's National Elites Foundation Research Award.



MO RASTGAAR (Senior Member, IEEE) received the B.S. degree in mechanical engineering from the Sharif University of Technology, Tehran, Iran, in 1995, the M.S. degree in mechanical engineering from Tehran Polytechnic, Iran, in 1998, and the Ph.D. degree in mechanical engineering from the Virginia Polytechnic Institute and State University, Blacksburg, VA, USA, in 2008. He was a Postdoctoral Associate with the Newman Laboratory for Biomechanics and Human Reha-

bilitation, Massachusetts Institute of Technology, Cambridge, MA, USA, from 2008 to 2010. From 2011 to 2018, he was an Assistant Professor and an Associate Professor with Michigan Tech, Houghton, MI, USA. In 2019, he joined Purdue University, West Lafayette, IN, USA, where he is currently a Professor with the Polytechnic Institute and the Director of the Human-Interactive Robotics Laboratory. His research interests include advancing maneuverability in lower extremity robotic prostheses and assistive robots by characterizing the agility in the human gait. He was a recipient of the 2014 National Science Foundation CAREER Award.